Design and error analysis of a high accurate star simulator based on optical splicing technology

LIU Zengyi[1,2,3], ZHAO Borui[1,2,3], XING Fei[1,2,3]

(1. *Department of Precision Instrument*, *Tsinghua University*, *Beijing* 100084, *China*;

2. *State Key Laboratory of Precision Measurement Technology and Instruments*, *Tsinghua University*, *Beijing* 100084, *China*;

3. *Collaborative Innovation Center for Micro/Nano Fabrication*, *Device and System*, *Tsinghua University*, *Beijing* 100084, *China*)

Abstract: Dynamic tar simulator has been widely used in calibration and validation for star trackers. To achieve both high accuracy and large view field, a dynamic star simulatorbased on optical splicing technology with 2 1920×1080−LCDs and a half−transmission and half−reflection prisms was proposed in this paper. The physical principal and error model due to the splicing structure has been discussed and analyzed in detail. Based on the Tsinghua Micro star tracker, the error effect and system accuracy has been carefully tested and calibrated. The result showed that this simulator can get the accuracy of 10.4" (3sigma) within a field of view of , which can meet the simulating requirement of modern star tracker, whose accuracy can reach 3" (3sigma)。

Key words: star Simulator; optical Splicing; seamless tiled, star tracker

1 Introduction

Star trackers, whose accuracy could reach arc second, are the most accurate attitude sensors available in space use. Due to the restriction of aerospace conditions, it´s almost impossible to test a star tracker in space. Therefore, ground experiment devices, star simulators, are designed to accomplish calibration and real time test for star trackers in lab conditions. Traditionally researchers used many other devices to test the performance of the star tracker. Reference [1] reports an optical calibration method of the star tracker based on a theodolite[2].

Star simulator simulates the brightness and location of the stars. As an optical simulation instrument, the accuracy, dynamic features and FOV are the key parameters of it so that many researchers take efforts to achieve a better performance. Reference[1] presents a star simulator with a LED board as its star map simulation system. This kind of system could achieve the dynamic simulation of the star map, but the error is only theoretically and briefly analyzed and no specific experiment results are given. Reference[2] reports the design of a static star simulator, mainly focused on the optical design and thermo analysis.

Although the accuracy could be improved, these approaches failed to figure out how to expand the FOV of the star simulator. The development of the tiled display technology provides a way to present high-resolution and large view-field images. Reference [3~5] summarized 6 different types of tiled display technology, like multi-monitors, tiled LCD panels and projector arrays etc. Reference [6~8] present 3 examples using multi-monitors and tiled LCD panels to display high-resolution images. But none of them tackle the top challenge in tiled display: the integration of the "tiles" to a seamless whole. Reference [9~12] provide some approaches to correct the color and the geometry, however, they just accomplish a rough calibration in order to make the images seem seamless which could not meet the requirement of the accuracy in the design of precision instruments.

Besides, since the study of enhancing the dynamic features of the star tracker is one of the top topics, the design of dynamic star simulator is becoming more and more attractive[13].

In this article, a high accurate and large view field dynamic star simulator based on optical splicing technology is described. We used optical splicing to solve the seam problem and the test result shows that the application of optical splicing technology in star simulator could achieve a good performance. Further, its error model established to provide a guidance of the manufacture and analysis of this kind of devices.

2 Design of the star simulator

2.1 Structure and working principle of the simulator

In order to expand FOV and achieve high accuracy, optical splicing is used to design the star simulator. It consists of 2 parts: the star map generation session and the optical collimating session. Figure 1 shows the structure of the whole system.

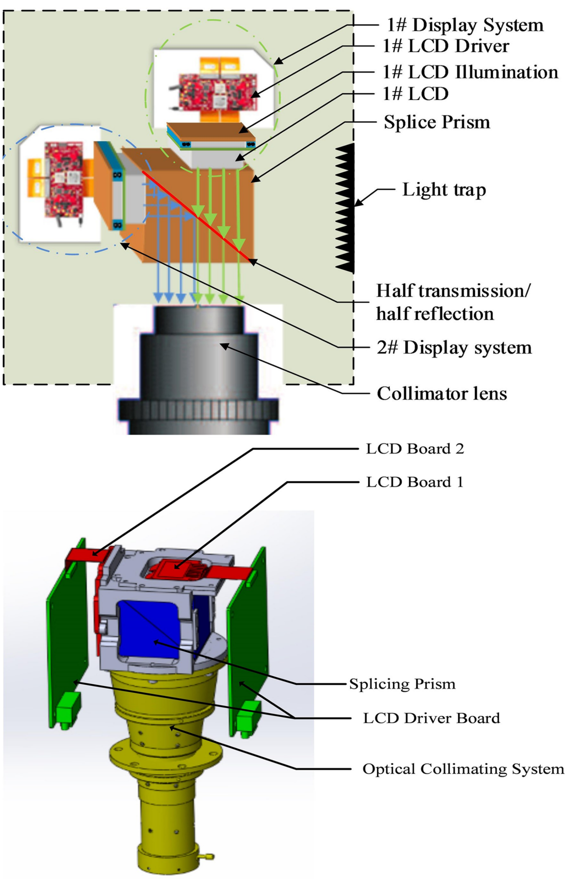

Fig. 1 Design of the Star Simulator Structure.
(a) Sketch of the star simulator;
(b) Design drawing of the star simulator.

Here is the working principle of the system, in the star map generation session, firstly a star map is split and displayed in the 2 LCD modulator boards, which are controlled by the computer and tightly fixed on the prism, and then the light radiated from the LEDs passes through them to the splicing prism. The prism is diagonal, therefore could put the 2 parts of the star map together to form the original one and the certain overlapping area is ensured by the structure of the frame. Meanwhile, the spliced image is located on the focal plane of the optical collimating system, thus the final image of the star map is infinity.

2.2 Star map generation algorithm

In order to achieve the simulation goal, the captured images simulated by star simulators should be coincided with the ones conjectured by the real space. Considering a star sensor working at attitude matrix A, the location of a real star can be described by an inertial vector

$$L = (v_x, v_y, v_z)^{\mathrm{T}} \tag{1}$$

Assuming that the error matrix between the CCD and the star sensor lens is A_s, the focal lengths of the star sensor is f_s and the coordinate of the original point is $(x_{0s}, y_{0s}, -f_s)$. Correspondingly, $(x_{0c}, y_{0c}, -f_c)$ represents coordinates of the original point and A_c represents the error matrix between the object plane and the lens of the star simulator.

Then according to the ideal pinhole model, the relation between the coordinates of the stars on the imaging plane and the object plane could be described as follow:

$$\frac{A_s L_s + (x_{0s}, y_{0s}, -f_s)^{\mathrm{T}}}{\| A_s L_s + (x_{0s}, y_{0s}, -f_s)^{\mathrm{T}} \|} = \frac{A_c L_c + (x_{0c}, y_{0c}, -f_c)^{\mathrm{T}}}{\| A_c L_c + (x_{0c}, y_{0c}, -f_c)^{\mathrm{T}} \|} = -AL \tag{2}$$

where

$$L_s = (x_s, y_s, 0)^{\mathrm{T}} \tag{3}$$

$$L_c = (x_c, y_c, 0)^{\mathrm{T}} \tag{4}$$

which represent the coordinates of the star on the object plane and image plane. Then using the equation (2), given the attitude matrix A, the error matrix A_c and the real star inertial vector, the coordinates of the star point in the star simulator could be calculated.

3 Error analysis of the spliced star simulator

3.1 Summary of the error sources of the spliced star simulator

The error of the simulation is inevitable due to the structure and composition of the system. According to the working process discussed above, the error of source of the system can be categorized as follows:

(1) *The star catalog error*

The star catalog error concerns the accuracy of the vector L in equation (2), and can be ignored when the catalog is checked before used.

(2) *The componential error*

The deformation and surficial inhomogeneity of each optical component could cause error. However, considering the manufacturing accuracy, the surficial inhomogeneity, which could reach few nanometers, can be ignored comparing to the other kinds of error. The deformation can be caused by the thermo-effects and the fabrication process. Here, in order to simplify the error propagation process, we assume that the deformation error only leads to the angle and location change of the corresponding plane, regardless of the non-planar error.

(3) *The optical collimating system error*

In order to achieve high accuracy, the image position precision of the optical collimating system must be accurate enough. According to reference [14], the error mainly results from the distortion of the optical system and is discussed specifically in Reference[15~17].

The error sources discussed above are often encountered and analyzed in the design of optical precision instruments. In this article, we will not study them deeply, instead we concern more about the error caused by the tiled display technology.

(4) *The positioning error between the components*

This error consists the positioning error between the LCD modulators and the prism and the one between the prism and the optical lens and could affect the error matrix A_c in equation (2). Besides, since the tiled display technology is used, the positioning error between the 2 LCD modulators will influence the accuracy of the whole system largely, so in the following discussion, we will focus on this kind of error.

3.2 Splicing display model of the simulator

Since the lacking of the study of the physical model of this kind of devices and its importance for the accuracy of the simulation result, it's essential to build the splicing display model of the simulator. In the follow analysis, we will mainly focus on the positioning error. Figure 2 shows the definition of the coordinate systems used below.

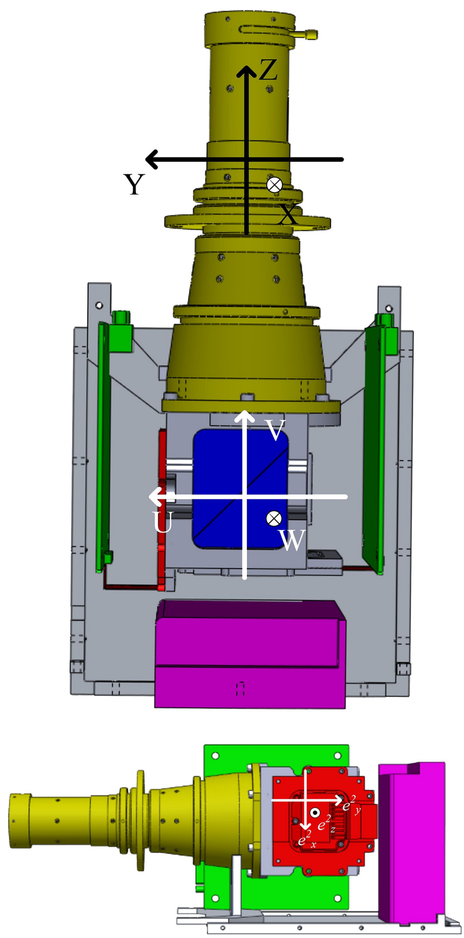

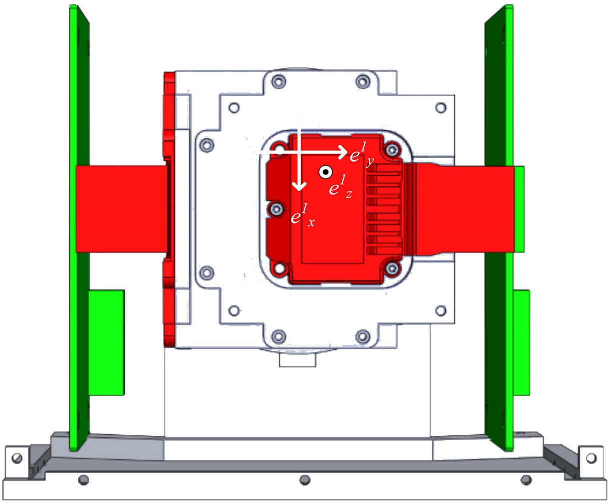

Fig. 2 Definition of the coordinate system.
(a) Definition of O-XYZ and O-UVW;
(b) (c) Definition of $O\text{-}e^1_x e^1_y$ and $O\text{-}e^2_x e^2_y$.

(1) As the optical collimating system can be simplified as a pinhole model, the frame O-XYZ is fixed on the optical principle point of the optical system and the axis OY is along with the principle axis. This coordinate system is used to present the imaging process.

(2) The frame O-UVW is fixed on the splicing prism, where axis OV is vertical to the surface of the prism. This coordinate system is used to elaborate the splicing process which mainly concerns about how the star map is formed by 2 LCD images and a half-transmission and half-reflection prism.

(3) The frame $O\text{-}e^1_x e^1_y e^1_z$ and $O\text{-}e^2_x e^2_y e^2_z$ is fixed on the corner of the LCD boards as shown in the figure which represent the drawing control system. The original points and axes $e^i_x, e^i_y, i = 1,2$ of this frame are also identical with the drawing control frames'. Since the LCDs are tight fixed on the splicing prism, the axes Oe^1_x, Oe^2_x and OW, Oe^1_z,-Oe^2_y and OU, $-Oe^1_y$, $-Oe^2_z$ and OV are in the same direction.

The error caused by the dislocation between LCDs and the prism could be described by the error matrices A_{P_i} which is specified as below.

$$A_{P_i} = \begin{pmatrix} \cos\mu_i\cos\omega_i & \sin\omega_i & \cos\omega_i\sin\upsilon_i & 0 \\ -\sin\mu_i\sin\upsilon_i - \cos\mu_i\cos\upsilon_i\cos\omega_i & \cos\mu_i\cos\omega_i & \cos\upsilon_i\sin\mu_i - \cos\mu_i\sin\upsilon_i\sin\omega_i & 0 \\ \cos\upsilon_i\sin\mu_i\sin\omega_i - \cos\mu_i\sin\upsilon_i & -\cos\omega_i\cos\mu_i & \cos\mu_i\cos\upsilon_i + \sin\mu_i\sin\upsilon_i\sin\omega_i & 0 \\ t_{\mu_i} & t_{\upsilon_i} & t_{\omega_i} & 1 \end{pmatrix}, i = 1,2 \tag{5}$$

where $\mu_i, \upsilon_i, \omega_i$ and $t_{\mu_i}, t_{\upsilon_i}, t_{\omega_i}$ respectively describe the angular error and transitional error of the LCDs in frame O-UVW.

Thus the coordinate conversion from the frame $O\text{-}e^i_x e^i_y e^i_z$ to the frame O-UVW should be

$$\begin{cases} L_{P_1} = A_{P_1}(A_{PL_1}L_{c_1} - \rho^1_{PL}) \\ L_{P_2} = A_{ref}A_{P_2}(A_{PL_2}L_{c_2} - \rho^2_{PL}) \end{cases} \tag{6}$$

Here L_{c_1} and L_{c_2} represent the star points' coordinates on LCDs. L_{P_1} and L_{P_2} represent the star points' coordinates after the splicing process. The ρ^1_{PL} and ρ^2_{PL} are used to present the vector pointing the original point of O-UVW respectively in $O\text{-}e^1_x e^1_y e^1_z$ and $O\text{-}e^2_x e^2_y e^2_z$. A_{PL_1} and A_{PL_2} represents the conversion matrix between $O\text{-}e^i_x e^i_y e^i_z$ and O-UVW where

$$A_{PL_1} = \begin{pmatrix} & -1 & & \\ & & -1 & \\ 1 & & & \\ & & & 1 \end{pmatrix} \tag{7}$$

$$A_{PL_2} = \begin{pmatrix} & & 1 & \\ & -1 & & \\ 1 & & & \\ & & & 1 \end{pmatrix} \tag{8}$$

A_{ref} stands for the process that the LCD2 is reflected where

$$A_{ref} = \begin{pmatrix} & -1 & & \\ -1 & & & \\ & & 1 & \\ & & & 1 \end{pmatrix} \tag{9}$$

After the splicing process, in order to form a full star map, there must be a certain overlapping area in the image formed by the splicing prism as shown in figure 3. Under ideal condition, the axis OV would pass through the center of the overlapping area as shown in figure 3.

Besides, the dislocation between the splicing prism and optical collimating system should also be included. Ideally, in the OXYZ system, the axes OV and OZ should be in the same direction and the rear surface of the prism should be positioned on the focal plane of the optical system. This kind of error could be described by the error matrix A_O between the prism and the optical system. The matrix A_O could be specified as below

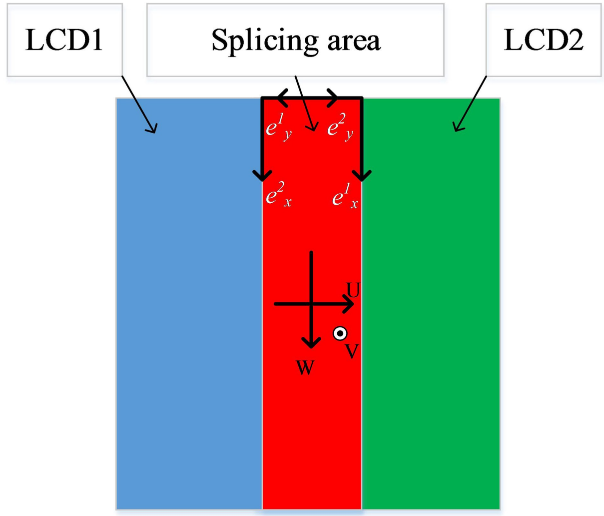

Fig. 3 The description of the ideal splicing process.

$$A_O = \begin{pmatrix} \cos\beta\cos\gamma & \sin\gamma & \cos\gamma\cos\beta & 0 \\ -\sin\alpha\sin\beta - \cos\alpha\cos\beta\sin\gamma & \cos\alpha\cos\gamma & \cos\beta\sin\alpha - \cos\alpha\sin\beta\sin\gamma & 0 \\ \cos\beta\sin\alpha\sin\gamma - \cos\alpha\sin\beta & -\cos\gamma\sin\alpha & \cos\alpha\cos\beta + \sin\alpha\sin\beta\sin\gamma & 0 \\ t_x & t_y & t_z & 1 \end{pmatrix} \tag{10}$$

Where α, β, γ respectively stand for the angles between axes OX and OW, OU and OY, OZ and OV and t_x, t_y, t_z represent the transition error of the splicing prism in frame O-XYZ.

Then the coordinates conversion between the frame O-UVW and O-XYZ is

$$L_{o_i} = A_O(A_{PO}L_{c_i} - \rho_{op}) \tag{11}$$

Where ρ_{op} is used to present the vector pointing the original point of the frame O-XYZ in frame O-UVW. A_{PO} represents the conversion matrix between O-UVW and O-XYZ where

$$A_{PO} = \begin{pmatrix} & 1 & & \\ 1 & & & \\ & & 1 & \\ & & & 1 \end{pmatrix} \tag{12}$$

Then the according to equation (6) and (11), the relation between the drawing frame coordinates and the lens frame coordinates is

$$\begin{cases} L_{O_1} = A_O A_{PO} A_{P_1} A_{PL_1} L_{c_1} - A_O A_{PO} A_{P_1} \rho^1_{PL} - A_O \rho_{OP} \\ L_{O_2} = A_O A_{PO} A_{ref} A_{P_2} A_{PL_2} L_{c_2} - A_O A_{PO} A_{ref} A_{P_2} \rho^2_{PL} - A_O \rho_{OP} \end{cases} \tag{13}$$

In practice, we used the LCD1 to display the splicing part as shown in figure 4. In order to deal with the splicing display process, the star map coordinate system $O\text{-}e_x e_y$ is defined and fixed on O-XYZ which is used to present the relation between the drawing of the star map and the computer drawing system. The left part of the star map relative to the split surface is displayed on LCD1 and the other part on LCD2.

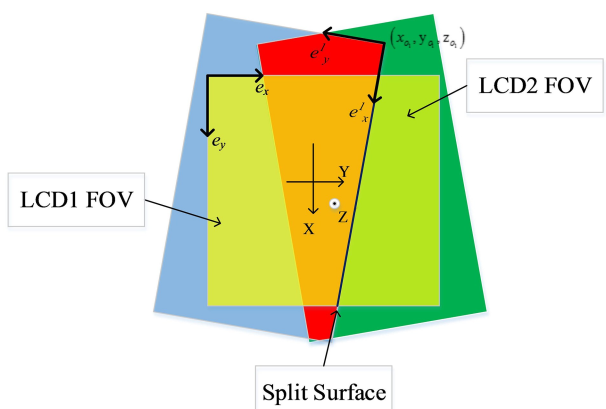

Fig. 4 The sketch of splicing display solution

Thus the split surface could be represented as

$$(L_{OS}-L_{OO})\bullet(A_O A_{PO} A_{P_1} A_{PL_1}\varepsilon_x^1 - A_O A_{PO} A_{P_1}\rho_{PL}^1 - A_O\rho_{OP}) = 0 \quad (14)$$

Where ε_y^1 represents the unit vector along e_y^1 in the frame $O\text{-}e_x^1 e_y^1 e_z^1$, $L_{OS}=(x,y,z,1)^T$ represents the coordinates of the points of the split surface in the frame $O\text{-}e_x e_y$, L_{OO} represents the coordinates of the original point of the frame $O\text{-}e_x^1 e_y^1 e_z^1$ and could be determined as below

$$L_{OO} = -A_O A_{PO} A_{P_1}\rho_{PL}^1 - A_O\rho_{OP} \quad (15)$$

Then according to equation (2) once a star described by attitude matrix A and location vector L is displayed on the simulator, the coordinates of the pixel which should be lighten could be presented by the equation below

$$\begin{cases} -AL = \dfrac{A_1 L_{c_1} - A_O A_{PO} A_{P_1}\rho_{PL}^1 - A_O\rho_{OP}}{\| A_1 L_{c_1} - A_O A_{PO} A_{P_1}\rho_{PL}^1 - A_O\rho_{OP} \|}, if(-AL-L_{OO})\bullet(A_1\varepsilon_y^1 - A_O A_{PO} A_{P_1}\rho_{PL}^1 - A_O\rho_{OP}) \geq 0 \\ -AL = \dfrac{A_2 L_{c_2} - A_O A_{PO} A_{ref} A_{P_2}\rho_{PL}^2 - A_O\rho_{OP}}{\| A_2 L_{c_2} - A_O A_{PO} A_{ref} A_{P_2}\rho_{PL}^2 - A_O\rho_{OP} \|}, if(-AL-L_{OO})\bullet(A_2\varepsilon_y^1 - A_O A_{PO} A_{P_1}\rho_{PL}^1 - A_O\rho_{OP}) < 0 \end{cases} \quad (16)$$

Where

$$\begin{cases} A_1 = A_O A_{PO} A_{P_1} A_{PL_1} \\ A_2 = A_O A_{PO} A_{ref} A_{P_2} A_{PL_2} \end{cases} \quad (17)$$

Then the according to equation (5) ~ (16), the splicing display model of the star simulator is fully established. Using the display equation (16), regardless of other sources of error, the devices could achieve an ideal simulation of the location of the star from infinity.

3.3 Parameter Simulation of the Simulator

Although the equation (16) provided a way to eliminate the error caused by the dislocation between the components, it's hardly to measure the factors in equation (5) and (8) precisely due to the restriction of the structure then it's essential to minimize the error during the manufacturing as much as possible. So we conducted a series of simulation to test the effect of each factor. The simulation parameters are shown in table 1.

Table 1 Simulation Parameters

Item	value	description
f_s	50mm	Focal length of the star tracker
l_p	50mm	Side length of the prism
l_{op}	173mm	The distance between the prism center and the optical center
δ_{LCD}	0.015mm	Side length of the LCD pixel
l_{LCD}	1920pixels	Length of the LCD board
w_{LCD}	1080pixels	Width of the LCD board

Here is the simulation process, firstly a series of star points are generated whose coordinates could be represented as L_0 (assuming that they are checked according to equation (16) and displayed on LCD1) and imaged under ideal condition as the standard imaging position whose coordinates could be represented as L_{std}. Then according to equation (2) and (13) considering the star tracker is under ideal condition, the relation between L_0 and L_{std} is

$$\frac{A_{PO}A_{PL_1}L_0 - A_{PO}\rho_{PL}^1 - \rho_{OP}}{\| A_{PO}A_{PL_1}L_0 - A_{PO}\rho_{PL}^1 - \rho_{OP} \|} = \frac{L_{std} + (0,0,-f_s)}{\| L_{std} + (0,0,-f_s) \|} \quad (18)$$

Where

$$\rho_{PL}^1 = \left(\frac{1}{2} l_{LCD}\delta_{LCD}, 0, -\frac{1}{2} l_p\right)^T$$

$$\rho_{OP} = (0, -l_{op}, 0)^T$$

Then the error factors are added and the imaging position L_{err} which contains error are calculated as followed

$$\frac{A_O A_{PO} A_{P_1} A_{PL_1} L_0 - A_O A_{PO} A_{P_1}\rho_{PL}^1 - A_O\rho_{OP}}{\| A_O A_{PO} A_{P_1} A_{PL_1} L_0 - A_O A_{PO} A_{P_1}\rho_{PL}^1 - A_O\rho_{OP} \|} = \frac{L_{err} + (0,0,-f_s)}{\| L_{err} + (0,0,-f_s) \|} \quad (19)$$

The difference $\delta_{err} = (L_{err} - L_{std})/f_s$ is used as the test result to evaluate the influence of each factor to the imaging process. The results are shown in figure 5 ~ 9.

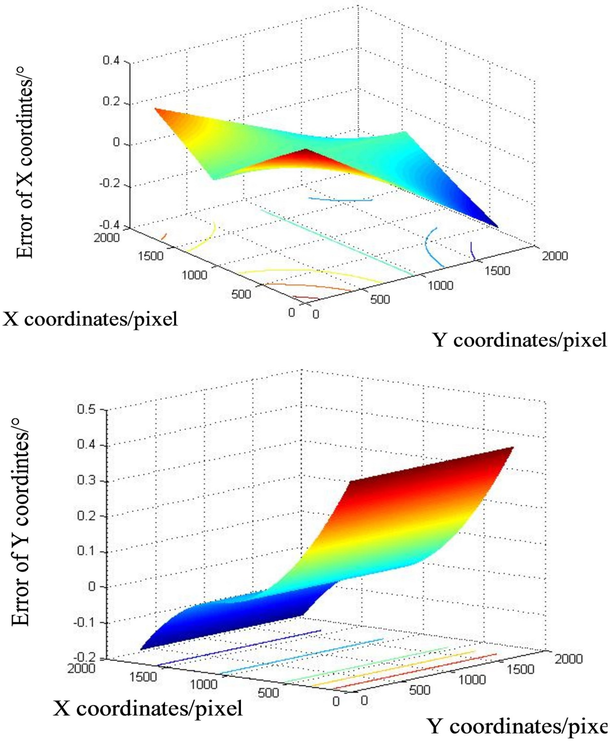

Fig. 5 The effects of $\mu_1 = 1°$ and $\mu_2 = -1°$.
(a) The error along X-axis. (b) The error along Y-axis.

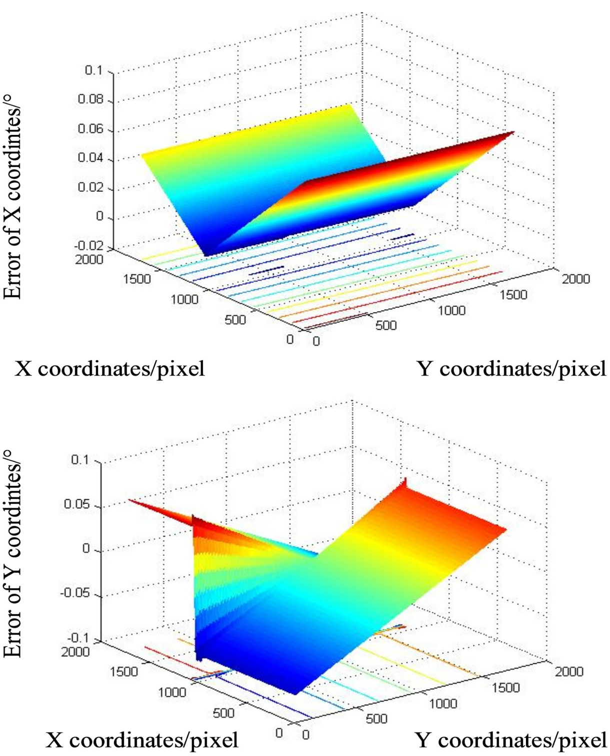

Fig. 6 The effects of $\upsilon_1 = 1°$ and $\upsilon_2 = -1°$.
(a) The error along X-axis. (b) The error along Y-axis.

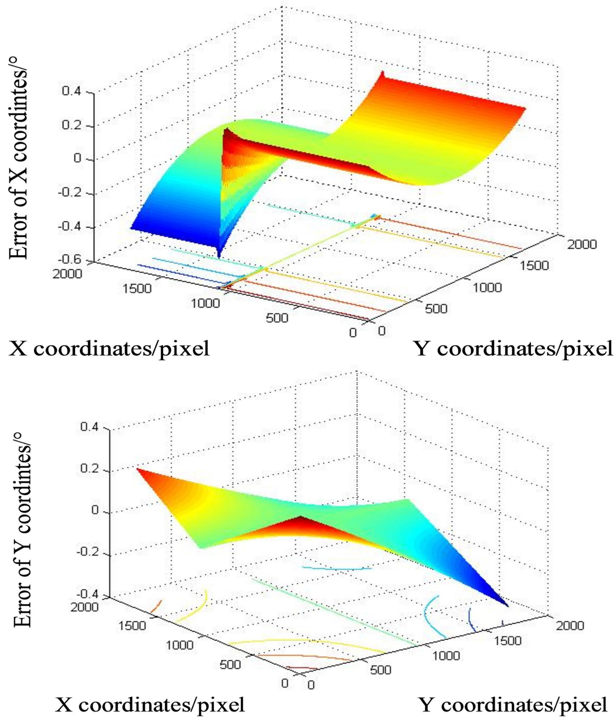

Fig. 7 The effects of $\omega_1 = 1°$ and $\omega_2 = -1°$.
(a) The error along X-axis. (b) The error along Y-axis.

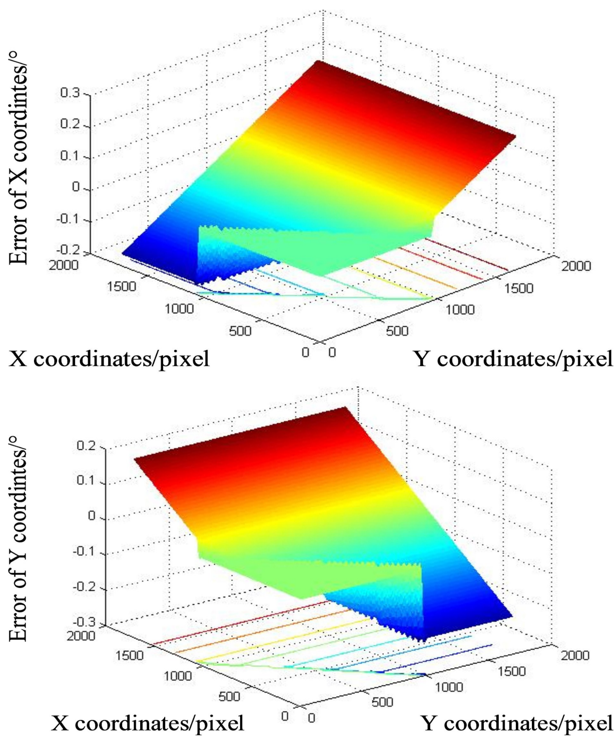

Fig. 8 The effects of $t_{\mu_1} = 10pixels$, $t_{\upsilon_1} = 10pixels$, $t_{\omega_1} = 10pixels$ and $t_{\mu_2} = 0$, $t_{\upsilon_2} = 0$, $t_{\omega_2} = 0$.
(a) The error along X-axis. (b) The error along Y-axis.

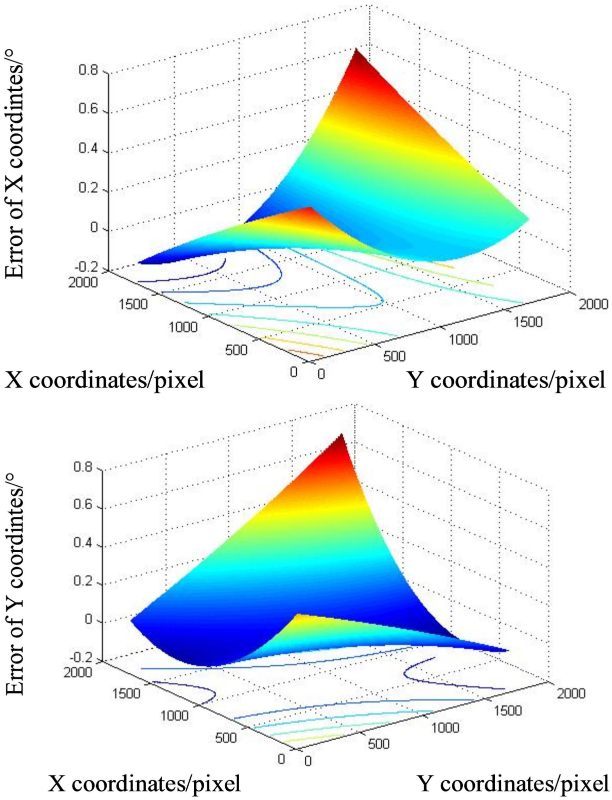

Fig. 9 The effects of $\alpha = 1°$, $\beta = 1°$, $\gamma = 1°$, $t_x = 10\ pixels$, $t_y = 10\ pixels$, $t_z = 10mm$.
(a) The error along X-axis. (b) The error along Y-axis.

The simulation results show that (1) a small dislocation between the components could cause huge error to the accuracy to the star simulator so that on the one hand, its essential to minimize the dislocation as much as possible during the manufacturing, on the other hand, the error calibration process is indispensable; (2) due to the restriction of the test method, the 18 effect factors could not be separate easily and since the optical distortion of the test system is inevitable, it's important to figure out a way to measure the factors.

4 Test of the effect factors

4.1 Test system and test method

In order to achieve the measurement of the effect factors and the evaluation of the performance of the device, we used a high-accurate star tracker whose accuracy could reach 2″. The real test scene is shown in figure 10.

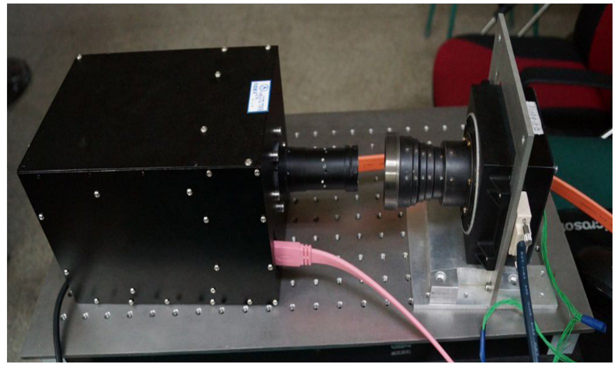

Fig. 10 Test scene of the simulator

Even though the optical system of the star simulator was designed to be distortion free, the distortion of the star tracker made it inappropriate to ignore the optical error of the test system. Since the distortion of the optical system is a function of the location, the test method is described as followed.

Firstly a set of star points formed a matrix are generated on the star simulator, and their location could be represented by L_{c_0} in the LCDs frame (here we use $L_{c_i} \in LCD1$ to present that L_{c_i} is still displayed on LCD1). Then the star tracker catches an image of the star points and their location could be presented by L_{s_0} in the star tracker frame. Here we use the following definition

$$f_1(L_c) = \frac{A_O A_{PO} A_{P_1} A_{PL_1} L_c - A_O A_{PO} A_{P_1} \rho^1_{PL} - A_O \rho_{OP}}{\| A_O A_{PO} A_{P_1} A_{PL_1} L_c - A_O A_{PO} A_{P_1} \rho^1_{PL} - A_O \rho_{OP} \|}$$

$$f_2(L_c) = \frac{A_O A_{PO} A_{P_2} A_{PL_2} L_c - A_O A_{PO} A_{P_2} \rho^2_{PL} - A_O \rho_{OP}}{\| A_O A_{PO} A_{P_2} A_{PL_2} L_c - A_O A_{PO} A_{P_2} \rho^2_{PL} - A_O \rho_{OP} \|}$$

The relation between L_{c_0} and L_{s_0} could be described as below

Where $\Delta_d(L_{s_0})$ represents the error caused by the optical distortion and e_{cs} represents the dislocation error vector between the star tracker and the star simulator. Then all the star points are moved i pixels along a certain direction and then represented by L_{c_i}. Correspondingly, the coordinates on the captured image of the star points could be represented by L_{s_i}, then their relation could be described by

$$g(L_{c_0}) = \begin{cases} f_1(L_{c_0}) = \dfrac{(L_{s_0} - \Delta_d(L_{s_0})) + (0,0,-f_s)}{\|(L_{s_0} - \Delta_d(L_{s_0})) + (0,0,-f_s)\|} + e_{cs}, if \quad L_{c_i} \in LCD1 \\ f_2(L_{c_0}) = \dfrac{(L_{s_0} - \Delta_d(L_{s_0})) + (0,0,-f_s)}{\|(L_{s_0} - \Delta_d(L_{s_0})) + (0,0,-f_s)\|} + e_{cs}, if \quad L_{c_i} \in LCD2 \end{cases} \tag{20}$$

$$g(L_{c_i}) = \begin{cases} f_1(L_{c_i}) = \dfrac{(L_{s_i} - \Delta_d(L_{s_0})) + (0,0,-f_s)}{\|(L_{s_i} - \Delta_d(L_{s_0})) + (0,0,-f_s)\|} + e_{cs}, if \quad L_{c_i} \in LCD1 \\ f_2(L_{c_i}) = \dfrac{(L_{s_i} - \Delta_d(L_{s_0})) + (0,0,-f_s)}{\|(L_{s_i} - \Delta_d(L_{s_0})) + (0,0,-f_s)\|} + e_{cs}, if \quad L_{c_i} \in LCD2 \end{cases} \tag{21}$$

According to equation (20) and (21), noticing that $L_{c_i} \approx L_{c_0}$ $L_{s_i} \approx L_{s_0}$, then $\Delta_d(L_{s_0}) \approx \Delta_d(L_{s_i})$ and

$$g(L_{c_i}) - g(L_{c_0}) = \frac{L_{s_i} - L_{s_0}}{\|(L_{s_i} - \Delta_d(L_{s_0})) + (0,0,-f_s)\|} \tag{22}$$

The equation (22) shows that, if we used $g(L_{c_i}) - g(L_{c_0})$ as the input of the test system and $L_{s_i} - L_{s_0}$ as the output, then the influence of the dislocation error e_{cs} and optical distortion error $\Delta_d(L_{s_0})$ could be significantly reduced.

Assume that equation (22) could also be written as

$$\varepsilon(L_{c_i}, L_{c_0}, A_O, A_{P_1}, A_{P_2}) = L_{s_i} - L_{s_0} \tag{23}$$

Thus, in practice, the effect factors of the system could be measured through the least square method described as below

$$\begin{cases} A_O = A_{Oe} \\ A_{P_1} = A_{P_1e} \\ A_{P_2} = A_{P_2e} \end{cases} \quad s.t. \ \|\varepsilon(L_{c_i}, L_{c_0}, A_O, A_{P_1}, A_{P_2}) - (L_{E_i} - L_{E_0})\| = \min \|\varepsilon(L_{c_i}, L_{c_0}, A_O, A_{P_1}, A_{P_2}) - (L_{E_i} - L_{E_0})\| \tag{24}$$

Where L_{E_i} and L_{E_0} represents the coordinates of the star points captured by the star tracker in experiments. Noticing that there are 18 effect factors, there are only 12 freedoms for the 2 LCDs so that there must be 6 coupling factors including 3 transitional and rotational factors. In order to focus on the splicing technology, we let $A_O = I$.

One problem about this differential method is that t_{μ_1}, t_{ω_1} and t_{μ_2}, t_{ω_2} stand for the in-plane transitional error of the 2 LCDs. It's easy to calculate that if L_{c_i} and L_{c_0} are always displayed on one LCD, then

$$\frac{\partial \varepsilon}{\partial \delta_i} = 0, \delta_i = t_{\mu_i}, t_{\omega_i}, i = 1,2$$

According to the section 3.3, t_{μ_i}, t_{ω_i} would influence the accuracy of the system. So it is important to let L_{c_i} and L_{c_0} be displayed on different LCDs. It could be accomplished if let the moving direction be vertical to the splicing edge and $L_{c_i} - L_{c_0}$ be large enough. In order to check if there are further parameter coupling, we use numerical analysis to do the examination. Define

$$\xi(A_{P_1}, A_{P_2}) = \|\varepsilon(L_{c_i}, L_{c_0}, I, A_{P_1}, A_{P_2}) - \varepsilon(L_{c_i}, L_{c_0}, I, I, I)\| \tag{25}$$

In the calculation, the simulation parameters are the same as in 3.3. Besides, $\|L_{c_i} - L_{c_0}\| = 20 pixels$ and the moving direction is vertical to the splicing edge to make sure that L_{c_i} and L_{c_0} are displayed on different LCDs. The result is shown in figure 11 ~ 16.

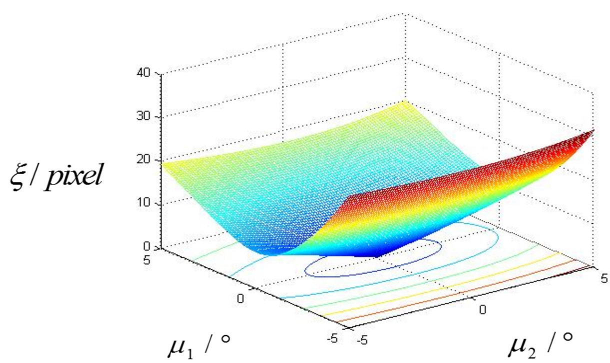

Fig. 11 The relation between $\xi(A_{P_1}, A_{P_2})$ and μ_1, μ_2

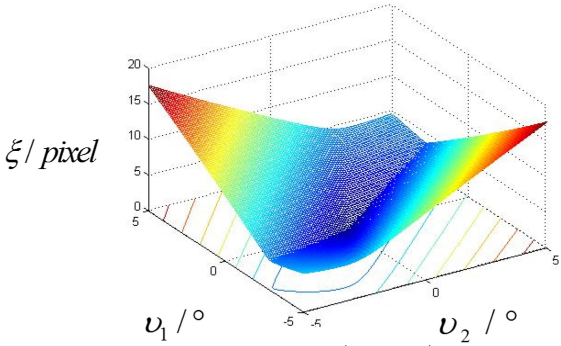

Fig. 12 The relation between $\xi(A_{P_1}, A_{P_2})$ and υ_1, υ_2

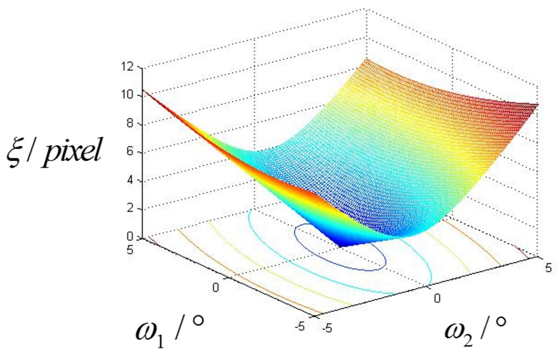

Fig. 13 The relation between $\xi(A_{P_1}, A_{P_2})$ and ω_1, ω_2

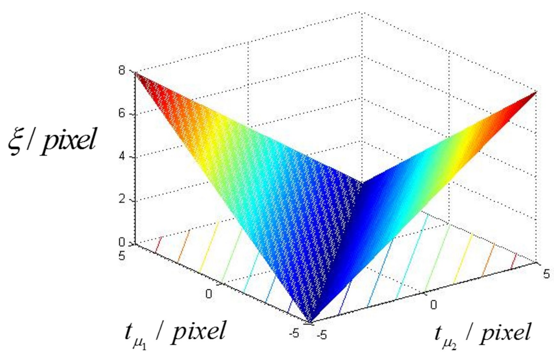

Fig. 14 The relation between $\xi(A_{P_1}, A_{P_2})$ and t_{μ_1}, t_{μ_2}

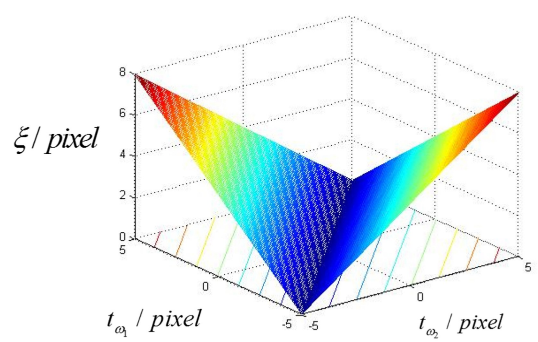

Fig. 15 The relation between $\xi(A_{P_1}, A_{P_2})$ and $t_{\omega_1}, t_{\omega_2}$

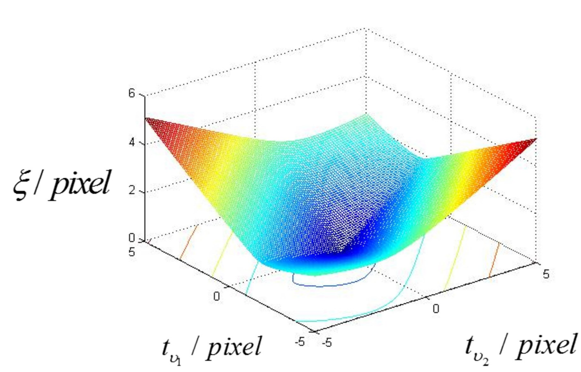

Fig. 16 The relation between $\xi(A_{P_1}, A_{P_2})$ and $t_{\upsilon_1}, t_{\upsilon_2}$

The numerical analysis shows that among the 12 factors, only t_{μ_1}, t_{μ_2} and $t_{\omega_1}, t_{\omega_2}$ are coupled respectively meanwhile other factors are not. So we let $t_{\mu_1} = 0, t_{\omega_1} = 0$ in the least square method.

4.2 Experiment process and result

The calibration experiment is conducted in the lab. In practice, we generated a phalanx-like star map containing 68 × 70 star points each time (the distance between points is 25 pixels) and their coordinates are recorded using the vector L_{c_i}. Then, in the captured image as shown in figure 12(a), the coordinates of the star points are determined by the gray value center of gravity and recorded using vector L_{E_i}. Here the subscript i stands for the number of the image. As shown in the figure 17(a), there is a seam between the 2 LCDs, so firstly a rough calibration is conducted by putting $t_{\mu_2} = 106, t_{\omega_2} = 32$ to make the star map seem seamless as shown in figure 17(b).

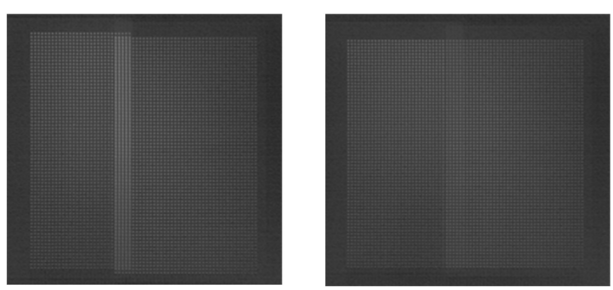

(a) (b)

Fig. 17 Image captured by the star tracker. (a) Original image. (b) Roughly calibrated image.

Even though the test method discussed in 4.1 has reduced the influence of optical distortion, the moving distance of each step could not be so long and the chosen star points to achieve the fitting process should be near the center of the FOV since the optical distortion is not removed entirely. So after the rough calibration, we let these points move 1 pixel a time and the moving distance is from 1 ~ 10 pixels then we get 11 images. After extracting the gray center of gravity, we found that in the 4^{th} image and the 6^{th} image, there are points move across the seam. In order to make sure that there are certain amount of points moving across the seam, we choose the star points in the 3^{rd} image as L_{E_0} and the 8^{th} image as L_{E_i} in equation (24). Using the test method discussed in section 4.1, we could get the fitting result as shown in table 2.

Table 2 Summarization of the effect factors

Item	Value
$\mu_1/°$	0.160744686
$\omega_1/°$	0.065374455
$\upsilon_1/°$	0.814493872
t_{υ_1}/mm	0.425189323
$\mu_2/°$	0.089786972
$\omega_2/°$	0.076919847
$\upsilon_2/°$	0.858602187
$t_{\mu_2}/pixel$	105.486252851
$t_{\omega_2}/pixel$	30.69484094
t_{υ_2}/mm	0.500015794

Using the test results in table 2, we could calculate the residual error after calibration and estimate the accuracy of the star simulator. Since the star simulator simulates the stars from infinite, the accuracy is defined as

$$e_c = \| \varepsilon(L_{c_i}, L_{c_0}, A_O, A_{P_1}, A_{P_2}) - (L_{E_i} - L_{E_0}) \| \times \frac{1}{\| L_{E_0} + (0,0,f_s)^T \|} \times \frac{3600 \times 180}{\pi} \quad (26)$$

The error distribution histogram and spatial distribution are shown in figure 18 and figure 19. The parameters of the simulator are summarized in table 3.

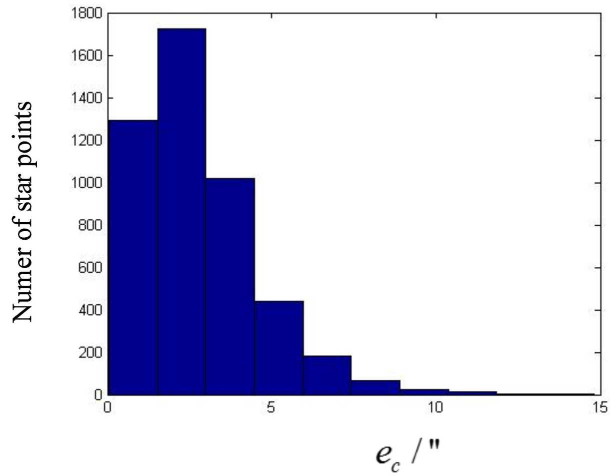

Fig. 18 Error distribution histogram

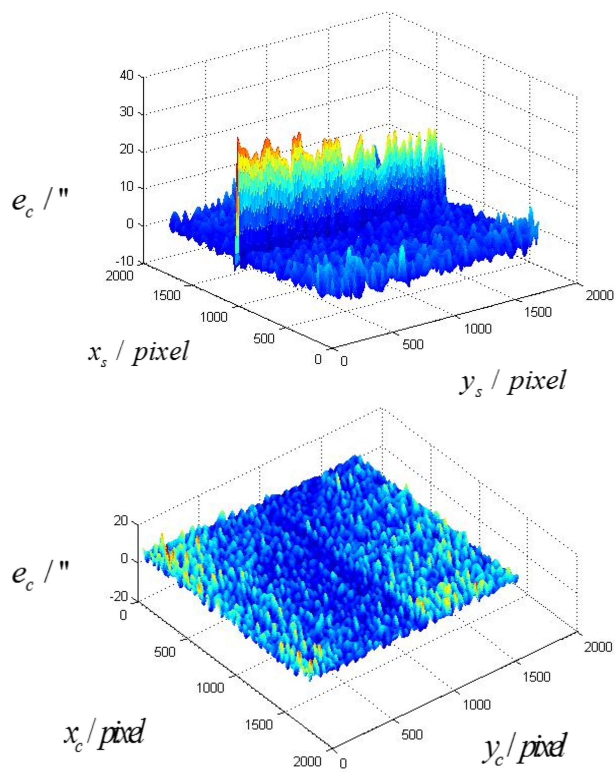

Fig. 19 Error spatial distribution.
(a) Before calibration. (b) After calibration.

Table 3 Summarization of the parameters

Parameter	Value
Field of view	≥ 8.1°
Position accuracy	≤10.45″(3σ)
Focal length	199.0156mm
Pixel size	0.015mm
Display resolution	2054 × 1889

We can see from figure 20 that after calibration, even though the star map is formed by 2 LCDs, the error caused by splicing edge is almost removed entirely. The spatial error distribution also shows that the error near the edge of the image is much higher than the center, which indicates that the error of optical distortion of the test system could not be fully reduced. Meanwhile, although we consider the star tracker as an ideal instruments, in fact, the error of the star tracker, like the electronic noise shown in figure 17, could still influence the test results like the error near the edge of the image. Even under such conditions, the position accuracy of the whole test system could reach $10.13''(3\sigma)$, which shows that the using the optical splicing technology, the goal of large FOV, high accuracy and dynamic display could be accomplished.

4 Conclusion

In this article, a novel star simulator based on tiled display technology has been proposed, its error model detailed and its performance tested. The experiment approach in this paper provide a way to measure the effect factors of this kind of devices avoiding the influence of the optical distortion. Based on this method, the performance of the simulator is tested and calibrated. The results show that the error propagation model and test method proved to be useful to remove the influence of the splicing seam. And they are also instructional to the design, manufacture, and measurement of this kind of devices. Finally, the performance test shows that the simulator fully achieve the goal of large FOV, high accuracy and dynamic display.

References

[1] SUN G, ZHANG G, WANG L, et al. Compact star simulator with very high accuracy[C]. 6th International Symposium on Advanced Optical Manufacturing and Testing Technologies (AOMATT 2012). International Society for Optics and Photonics, 2012: 84171J-84171J-4.

[2] GUO-YU C Q Z, LING-YUN W Z W, YU-JUN G. Design of static star simulator based on testing of very high accuracy star sensor[C]. Proc. of SPIE Vol. 2013, 8907: 890707-1.

[3] HERELD M, JUDSON I R, STEVENS R L. Introduction to building projection-based tiled display systems [J]. Computer Graphics and Applications, IEEE, 2000, 20(4): 22-28.

[4] HERELD M, JUDSON I R, PARIS J, et al. Developing tiled projection display systems[C]. Proc. IPT 2000 (Immersive Projection Technology Workshop). 2000.

[5] NI T, SCHMIDT G S, STAADT O G, et al. A survey of large high-resolution display technologies, techniques, and applications[C]. Virtual Reality Conference, 2006. IEEE, 2006: 223-236.

[6] BROWN M S, SEALES W B. A practical and flexible tiled display system[C]. Computer Graphics and Applications, 2002. Proceedings. 10th Pacific Conference on. IEEE, 2002: 194-203.

[7] DAVIS J, CHEN X. Lumipoint: Multi-user laser-based interaction on large tiled displays[J]. Displays, 2002, 23(5): 205-211.

[8] KRUMBHOLZ C, LEIGH J, JOHNSON A, et al. Lambda table: high resolution tiled display table for interacting with large visualizations[C]. Proceedings of 5th Workshop on Advanced Collaborative Environments, Redmond, Washington. 2005.

[9] YA-HUI L, QING-XUAN J, HAN-XU S, et al. A geometry calibration and visual seamlessness method based on multi-projector tiled display wall[C]. Informatics in Control, Automation and Robotics, 2009. CAR '09. International Asia Conference on. IEEE, 2009: 450-453.

[10] MAJUMDER A, HE Z, TOWLES H, et al. Achieving color uniformity across multi-projector displays[C]. Visualization 2000. Proceedings. IEEE, 2000: 117-124.

[11] BINNS J, GILL G, HERELD M, et al. Applying geometry and color correction to tiled display walls[C]. IEEE Visualization. 2002.

[12] LI Z, VARSHNEY A. A real-time seamless tiled display system for 3D graphics[C]. Immersive Projection Technology Symposium of the IEEE Virtual Reality 2002 Conference (VR2002 IPT). 2002.

Authors' Biographies

LIU Zengyi, born in 1983, is currently a Postgraduate Student in the Department of Mechanical Engineering, Tsinghua University, China. He obtained his Bachelor degree from Northwestern Polytechnical University in 2008. His major interests include Nano star tracker and Pico star tracker technology, etc.

Email: liuzengyi@mail.tsinghua.edu.cn

ZHAO Borui, born in 1991. He obtained his Bachelor degree from Department of Precision Instruments, Tsinghua University. His major interests include celestial navigation, high precision star tracker technology, etc.

Email: boruizhao@163.com

XING Fei, born in 1979, is currently an associate professor in Tsinghua University, China. He received his Bachelor degree from Tongji University in 2002 and Ph.D. degree from Tsinghua University in 2007. His current research interests focus on advance optical attitude sensor for space, remote sensing and celestial navigation.

Email: xingfei@tsinghua.edu.cn